Nonlinear Finite Element Analysis of Reinforced Concrete Arched Beams with Normal and High Compressive Strength

Dr. Haider Kadhim Ammash
Engineering College, University of Al-Qadisiya /Baghdad
Email:amashhk@gmail.com

Received on:11/10/2011 & Accepted on:10/1/2013

ABSTRACT

This study describes a three-dimensional nonlinear finite element model suitable for the analysis of high strength reinforced concrete arched beams under static load. The twenty node isoperimetric brick element has been used to model the concrete and reinforcing steel bars have been idealized as axial members embedded within the brick elements. Perfect bond was assumed to occur between the concrete and the reinforcing bars. The behavior of concrete in compression is simulated by an elasto-plastic work hardening model followed by a perfectly plastic response, which is terminated at the onset of the crushing. In tension, a smeared crack model with fixed orthogonal cracks has been used. High and normal strength reinforced concrete arched beams have been analyzed in the present study. Parametric studies have been carried out to investigate the effect of radius to span length ratio, boundary conditions**,** (α_2) [the sudden loss of stress at the instant of cracking], and effect of compressive strength**.** In general good agreement between the finite element solutions and the experimental results have been obtained.

Keywords: Reinforced Concrete Arched Beam, High Strength Concrete, Finite Element Method.

التحليل اللاخطي بالعناصر المحددة للعتبات الخرسانية المسلحة المقوسة مع مقاومة إنضغاط عادية وعالية

الخلاصة

تصف هذه الدراسة إنموذجاً لا خطياً ثلاثي الأبعاد بطريقة العناصر المحددة لتحليل العتبات الخرسانية المسلحة المقوسة .تم استخدام العنصر الطابوقي الثلاثي ذو العشرين عقدة لتمثيل الخرسانة. أما حديد التسليح فقد تم تمثيله باستخدام عنصر أحادي البعد(محوري) مطمور في عنصر الخرسانة مع افتراض وجود ترابط تام بين الخرسانة وحديد التسليح. تم تمثيل تصرف الخرسانة تحت اجهادات الضغط باستخدام النموذج المرن-اللدن ذو التقوية الانفعالية والمتبوع بتصرف لدن تام يستمر لغاية أقصى انفعال انضغاط تتهشم عنده الخرسانة. أما تحت تأثير إجهادات الشد فقد تم تبني نموذج التشقق المنتشر . في هذه الدراسة تم تحليل العتبات الخرسانية المسلحة المقوسة ذات المقاومة العالية وأخرى ذات مقاومة عادية،كما تم فحص تأثير

https://doi.org/10.30684/etj.2013.82186
2412-0758/University of Technology-Iraq, Baghdad, Iraq

نسبة تقوس إلى طول العتب، ظروف الإسناد، ($\alpha_{٢}$)،ومقاومة الانضغاط للخرسانة. وقد وجد بصورة عامة أن التحليل اللاخطي ثلاثي الأبعاد يعطي توافقاً جيداً مع النتائج العملية.

Notations

The following symbols are used in this paper

C_p = Plasticity coefficient
E_c = Modulus of elasticity of concrete
E = Modulus of elasticity of steel reinforcement
f = Yield function
I_1 = First stress invariant
J_2 = Second deviatric stress invariant
N_i = Shape function of node i of the brick element
u,v,w = Displacement components in the x,y and z-direction
X,Y,Z = Global coordinate system
c = Matreial constant
β = Shear retention factor or material constant
σ_n, σ_c = Stress
σ_o = Effective stress at onset of plastic deformation
σ_{cr} = Cracking stress
ε_n, ε_c = Strain
ε_{cu} = Concrete ultimate strain
ε_o = Strain corresponding to peak uniaxial concrete compressive stress
ε_{cr} = Cracking strain
γ_1, γ_2, γ_3 = Shear retention parameters
ξ,η,ζ = Local coordinate system

INTRODUCTION

In the past, the arches represent one of the few structural systems which make it possible to cover large spans. The earliest inhabitants developed the arch as an important element of their architecture as expressed by remaining bridges, aqueducts, and large public buildings. Today, the same importance is presented especially in bridge construction. The main aim of the arch is to enhance the load carrying capacity which may come from the stiffening behavior due to membrane action. Deep arches cause less thrust than flat ones, but they exhaust more material to cover the same span [3].

A number of investigators have studied experimentally the in plane nonlinear behavior and buckling of shallow arches. Jain (1960)[11] presented a method for the analysis of reinforced concrete arches taking into account the effect of plastic deformations. Elastic-perfectly plastic stress-strain relationship was adopted. The theoretical results were verified by test results. The in-plane buckling of sinusoidal shallow arches was studied by Timoshenko and Gere (1961)[19], and by Simitses (1976)[18]. Gjelsvik and Bodner (1962)[7] investigated the instability of fixed, shallow circular arches subjected to a central point load. Their theoretical modeling was based on an energy method, and they carried out an experimental study on aluminum alloy arches. Schreyer and Masur (1966)[17] performed an exact analysis for shallow circular arches subjected to radial pressure and derived analytical solutions, but their analysis was limited to fixed arches with a rectangular solid

section and their solutions were very complicated. Dickie and Broughton (1971)[6] used a series method to study the buckling of pin-ended and circular arches, and approximate numerical solutions were given, as well as the results of a series of tests carried out on Perspex arches. More recently, Hadi (2002)[9] drive and use the arched beam finite element in the analysis of reinforced concrete arches. The strain energy principle is used to formulated the stiffness matrix. Rubin (2004)[16] used the Cosserat theory to predict the buckling load and deformed shapes of elastic clamped circular arches and arched elastic rods. Wang et al. (2007)[21] presents an experimental investigation of two shallow reinforced concrete tied arches on roller supports, which were loaded to failure under short-term loading so that the effects of shrinkage and creep deformations were not significant. These tests provide bench mark validations for theoretical studies, and those of the companion paper Bradford et al. (2006)[3] are shown in particular to agree well with the test results reported there.

FINITE ELEMENT ANALYSIS OF REINFORCED CONCRETE

Three–Dimensional Brick Element:

Shape Functions:

The element has twenty nodes and sixty degrees of freedom and bounded by planes with ξ, η, and ζ = ± 1 in ξ, η, ζ space. The starting point for the stiffness matrix derivation is the element displacement field. The isoparametric definition of displacement components is:

$$\left.\begin{aligned} u(\xi,\eta,\zeta) &= \sum_{i=1}^{n} N_i(\xi,\eta,\zeta)\, u_i \\ v(\xi,\eta,\zeta) &= \sum_{i=1}^{n} N_i(\xi,\eta,\zeta)\, v_i \\ w(\xi,\eta,\zeta) &= \sum_{i=1}^{n} N_i(\xi,\eta,\zeta)\, w_i \end{aligned}\right\} \quad \text{...(1).}$$

Where:

N_i (ξ, η, ζ) is the shape function at the i-th node and u_i, v_i and w_i are the corresponding nodal displacements. The shape functions of the quadratic twenty node brick element are shown in Table (1).

STRAIN AND STRESS FIELDS

Since the geometrical nonlinearities are not considered in the present work, displacement gradients remain small throughout the loading process and hence the engineering components of strain can be expressed in terms of the first partial derivatives of the displacement components. Therefore, the linearized strain–displacement relationships may be written as:

$$\{\varepsilon\} = \begin{Bmatrix} \varepsilon_x \\ \varepsilon_y \\ \varepsilon_z \\ \gamma_{xy} \\ \gamma_{yz} \\ \gamma_{zx} \end{Bmatrix} = \begin{Bmatrix} \frac{\partial u}{\partial x} \\ \frac{\partial v}{\partial y} \\ \frac{\partial w}{\partial z} \\ \frac{\partial u}{\partial y} + \frac{\partial v}{\partial x} \\ \frac{\partial v}{\partial z} + \frac{\partial w}{\partial y} \\ \frac{\partial w}{\partial x} + \frac{\partial u}{\partial z} \end{Bmatrix} = \sum_{i=1}^{20} \begin{bmatrix} \frac{\partial Ni}{\partial x} & 0 & 0 \\ 0 & \frac{\partial Ni}{\partial y} & 0 \\ 0 & 0 & \frac{\partial Ni}{\partial z} \\ \frac{\partial Ni}{\partial y} & \frac{\partial Ni}{\partial x} & 0 \\ 0 & \frac{\partial Ni}{\partial z} & \frac{\partial Ni}{\partial y} \\ \frac{\partial Ni}{\partial x} & 0 & \frac{\partial Ni}{\partial z} \end{bmatrix} \cdot \begin{Bmatrix} u_i \\ v_i \\ w_i \end{Bmatrix} \quad \text{...(2)}$$

where:
[B] is Strain – displacement matrix
Since the shape functions Ni are functions of the local coordinates rather than Cartesian coordinates, a relationship needs to be established between the derivatives in the two coordinates systems.
The vector of stresses is given by:

$$\{\sigma\} = \begin{Bmatrix} \sigma_x \\ \sigma_y \\ \sigma_z \\ \tau_{xy} \\ \tau_{yz} \\ \tau_{zx} \end{Bmatrix} \quad \text{...(3)}$$

and the stress – strain relationship is represented as:

$$\{\sigma\} = [D] . \{\varepsilon\} \quad \text{...(4)}$$

where:
[D] is the constitutive matrix.

ELEMENT STIFFNESS MATRIX

The tangential stiffness matrix of the three-dimensional isoparametric solid element is given by:

$$[K]^e = \int_{V^e} [B]^T . [D] . [B] \, dv^e \quad \text{...(5)}$$

By using the transformation product rule, the stiffness matrix becomes:

$$[K]^e = \int_{-1}^{+1} \int_{-1}^{+1} \int_{-1}^{+1} [B]^T [D] [B] |J| d\xi d\eta d\zeta \quad \text{...(6)}$$

Where:
[J] is the Jacobian matrix and the elements of this matrix can be obtained by differentiation of equation (1).

THE OBSERVED BEHAVIOR OF NSC AND HSC

Concrete has a highly heterogeneous internal structure. It contains three different phases, the hydrated cement paste (HCP), the aggregate, and the transition zone between the cement paste and the aggregate. The aggregate phase is responsible for the unit weight, and elastic modulus being generally stronger than

the other two phases of concrete. The aggregate phase has no direct influence on the strength of concrete. The hydrated cement paste develops as a result of chemical reactions between the cement minerals and water. Many solids are produced as a result of this reaction and in addition to the solids; HCP contains several types of voids, which have an important influence on its properties. The third phase of concrete is the transition zone, which is produced from the result of chemical reactions between cement and water in the vicinity of the coarse aggregate particles. The strength of the transition zone at any point depends on the volume and size of voids present and on the presence of microcracks even before the structure is loaded. The transition zone will be susceptible to cracking when subjected to the influence of tensile stresses induced by differential movements between the aggregate and the HCP. Presence of transition zone has a great influence on the tensile and compressive strength and on the modulus of elasticity [13]. Normal strength concrete (NSC) made with cement and conventional natural aggregate suffers from several deficiencies. To overcome these deficiencies, many types of concrete have been developed. One of these is the high strength concrete (HSC). High strength concrete is defined as that having a compressive strength in the range from 41 to 83 MPa[1]. The porosity of the three phases of concrete is the most important strength determining factor in HSC. It appears that the water cement ratio holds the key to the porosities of both the HCP and the transition zone [14]. For the production of HSC, the opposing effects of water-cement ratio on consistency and strength of concrete cannot be harmonized without the use of water-reducing admixtures.

Despite the fact that few codes provide any design rules (15) for concrete strength greater than 50 MPa, the major difference between the NCS and the HSC is that HSC tends to behave as elastic and more brittle material compared with NSC. Therefore a great need exists for investigating HSC prior to its use in every day constructions. HSC properties such as stress-strain relationship, modulus of elasticity; tensile strength and Poisson's ratio are reviewed in the following sections.

UNIAXIAL BEHAVIOR OF CONCRETE

Stress-Strain Behavior in Uniaxial Compression:

Axial stress versus strain curves for concrete of compressive strength up to 67MPa is shown in Figure (2). The shape of the ascending part of the stress-strain curve is more linear and steeper for high strength concrete, and the strain at the maximum stress is slightly larger for high strength concrete[1, 4,20]. The slope of the descending part becomes steeper for HSC compared with NSC.

HSC exhibits less internal micro cracking than lower strength concrete for a given imposed axial strain [4]. As a result, the relative increase in lateral strain is less for high strength concrete, Figure (2). The lower relative lateral expansion during the inelastic range may mean that the effects of triaxial stresses will be proportionally different for HSC compared with NSC.

MODULUS OF ELASTICITY

A comparison of experimentally determined values for the modulus of elasticity with those predicted by the expression given by ACI Building Code[10] 318M-95 for NSC, based on a dry unit weight (2346 kg/m^3) is given in Figure (3).

$$E_c = 4700\sqrt{fc'} \qquad \text{...(7)}$$

This expression overestimates the modulus of elasticity for concrete with a compressive strength over 41MPa for the data given in Figure (3).

A correlation between the modulus of elasticity E_c and the compressive strength $f'c$ for normal weight concrete as shown in Figure (3), was reported as [1]:

But for compressive strength of concrete ($\mathbf{21MPa \le f'c \le 83MPa}$)

$$E_c = 4700\sqrt{fc'} + 6900 \qquad \text{...(8)}$$

Equation (13) is a better correlation between the modulus of elasticity and the compressive strength [1] of HSC.

Poisson's Ratio:

Experimental data on values of Poisson's ratio for **HSC** are very limited. Carrasquillo et al [14] reported values for Poisson's ratio of concrete having uniaxial compressive strengths up to 73 MPa to be 0.2 regardless of compressive strength. Many researchers [1] reported values for Poisson's ratio of **HSC** ranging from 0.2 to 0.32, while for NSC, a value ranging from 0.15 to 0.22 was achieved. In the present work Poisson's ratio assumed to be 0.17 for both NSC and HSC.

UNIAXIAL TENSION BEHAVIOR OF CONCRETE

Available information on the complete load-deformation response of concrete subjected to uniaxial tension is scarce and conflicting [8]. Since the direct tension test of concrete is complex and needs a special technique, indirect tensile test (cylinder splitting test) is usually used to determine the tensile strength of concrete. Many researchers [1] studied the relationship between the tensile strength and the compressive strength of concrete having compressive strengths of up to 83.8MPa. It was found that the tensile strength usually ranges from 0.05 of compressive strength for HSC to more than 0.1 of compressive strength for NSC. The following equation was reported for prediction of the tensile splitting strength (f_{sp})[1, 4]

$$f_{sp} = 0.59\sqrt{f_c'} \qquad \text{MPa} \qquad \text{...(9)}$$

MODELING OF MATERIAL PROPERTIES

The material model used in the present work is suitable for the three-dimensional nonlinear analysis of reinforced concrete structures under monotonically increasing load. The behavior of concrete in compression is presented by an elastic-plastic strain hardening model followed by a perfectly plastic response, which is terminated at the initiation of crushing. The growth of subsequent loading surfaces is described by an isotropic hardening rule. A parabolic equivalent uniaxial stress-strain curve shown in Fig (4) has been used to represent work hardening stage of behavior and the plastic straining is controlled by an associated flow rule. A yield criterion suitable for analyzing reinforced concrete members has been used. This criterion was used successfully can be expressed as:

$$f(\{\sigma\}) = c\, I_1 \left[(c\, I_1)^2 + 3\beta J_2 \right]^{1/2} = \bar{\sigma} \qquad \text{...(10)}$$

Where:

c and β are material parameters to be determined by fitting biaxial test results. Using the uniaxial compression test and the biaxial test under equal compressive stresses. I_1 and J_2 are the first stress and second deviatoric stress invariants and σ_0 is the equivalent effective stress taken from uniaxial tests.

In tension, linear elastic behavior is assumed to occur prior to cracking. Crack initiation is controlled by a maximum tensile stress criterion. A smeared crack model with fixed orthogonal cracks has been adopted to represent the behavior of cracked sampling points. The retained post-cracking tensile stress and the reduced shear modulus are calculated according to Figure (5) and (6) respectively.

MODELING OF REINFORCEMENT

A bilinear uniaxial stress-stain relationship is used for steel reinforcement as shown in Figure (7). Elastic unloading is also included. For the calculation of stresses at the loading stage, the following equations are used[23]:

$$f_s = E_s(\varepsilon_s - \varepsilon_{pi}) \text{ for } f_s \le f_{yi} \qquad \text{...(11)}$$

$$f_s = E_w/E_s\,(f_{s'} - f_{yi}) + f_{yi} \text{ for } f_s > f_{yi} \qquad \text{...(12)}$$

Where

$$f_{s'} = E_s\,(\varepsilon_s - \varepsilon_{pi}) \quad \text{for } f_s > f_{yi} \qquad \text{...(13)}$$

Where

f_s = Uniaxial stress of steel at strain ε_s.
f_{yo} = Initial yield stress of steel .
f_{yi} = Current yield stress of steel .
E_s = Modulus of elasticity for steel.
E_w = Hardening modulus of steel.
ε_{yo} = Initial yield strain of steel, and
ε_{pi} = Permanent plastic strain at currently yield stress.

OUTLINE OF COMPUTER PROGRAM

The computer program 3DNFEA (3-Dimensional Nonlinear Finite Element Analysis) has been used in the present study. This program has been originally developed by Al-Shaarbaf and introduced in his Ph.D thesis [2]. In the current research work, The computer program has been generalized to deal with high strength concrete as well as normal strength concrete arched beams. The main objective of the program is to analyze reinforced concrete members under general three-dimensional states of loading up to failure. The program was coded in FORTRAN-77 language and has been implemented an Amdahl 5980-300E main frame computer. In the present study, the program had been proceed using personal computer. The new MICROSOFT FORTRAN Power station 4.0 compiler, which becomes available in the late 1998, has been used. The modified program is suitable for analyzing high strength reinforced concrete arched beams under general states of loading.

NUMERICAL APPLICATIONS

In order to ensure the efficiency and the accuracy of the proposed method of analysis, two beams are studied and compared with test result.

Simply supported reinforced concrete arched beam with Subtended Angle 87.24º (Example No. 1):

A simply support reinforced concrete arched beam is analyzed using computer program (***3DABA***). A beam was tested by **Jain** [11], the beam has a total length (3.05 m) with cross-sectional dimensions (100 mm × 100 mm). It has no web reinforcement and the longitudinal reinforcement consists of one bar with a total area of (64.5 mm^2) in tension and compression. The beam subjected to concentrated load at L/4 of span, as shown in Fig (6-a).

The beam is modeled by (٨) brick elements of 20-noded, Figure (6-b) shows the details of the finite element mesh for the beam. The Material properties of concrete and steel are given in Table (2).

Hadi [9] solved this example using the elastic and elastic-plastic analysis of reinforced concrete frames 12 straight beam elements.

The load-deflection response at point load of the beam and a comparison of the calculate deflection with the previous study of Hadi [9].is shown in Figure (7). The computed deflection and load failure show good agreement with the experimental results for most loading levels.

Roller-pin supported reinforced concrete arched beam with subtended Angle 22.8º (Example No. 2):

A roller-pin Supported reinforced concrete arched beam has a cross section of (500 mm × 50 mm) was tested under a uniform load by Wang ET. Al [21] (2007). The reinforcement details are provided in Figure (8-a), this figure shows also the details of the beam geometry. Concrete and steel properties and additional material parameters are given in Table (3).

This beam was divided into (20) brick elements. Another finite element mesh has also been used to assess the accuracy of the finite element model. This mesh consisted of (16) brick elements. Figure (8-b) and Figure (8-c) show the details of the finite element mesh. The load-deflection curves of the beam at mid span point are shown in Figure (9). Results of the finite element analysis give good agreement with the experimental results of Wang et. al[21].

Bradford et al. 2007[3] solved this example dependent on the slenderness parameter λ given by $\lambda = \frac{2f}{r_x}$, in which r_x = major axis radius of gyration, and on the dimensionless ratio α of the axial stiffness AE/L of the arch to the stiffness k of each elastic horizontal spring support defined by,

$$\alpha = 2\frac{AE}{kL} = \frac{AE}{A_t E_t} \qquad \text{...(14)}$$

Where:

E=elastic modulus of the arch beam; A=transformed cross sectional area of arch beam, and E_T and at =corresponding values for the tie.

$$q = \left[0.26 \pm 0.74\left(1 - \left(0.63\pi^4(1+\alpha)/\lambda^2\right)^{1/2}\right)\frac{32\pi^2 EIf}{L^4} \right] \qquad \text{...(15)}$$

Where:

I=second moment of area of the transformed cross section of the arch about its major axis.

The theoretical treatment also derived the deflection of the crown of the arch under a uniformly distributed load (***q***) to be as:

$$v_c = \frac{2\omega f}{\theta^2\left[\sec(\theta) - 1 - \frac{\theta^2}{2}\right]}$$

in which

$$\theta = \frac{\mu L}{2}, \omega = \frac{qp - N}{N} \quad \theta = \mu L/2$$

$p = \frac{L^2}{8f} =$ focal parameter for a parabola

$\mu^2 = \frac{N}{EI} =$ familiar stability parameter

N= actual axial force in the arch

Parametric Study

Example No.1 is chosen to study the influence of some parameters that affect the behavior of reinforced concrete arched beam under static load. These parameters include the effect of radius to span-length ratio, effect of boundary conditions, effect (α_2) [the sudden loss of stress at the instant of cracking], and effect of compressive strength. The arched beam was divided to ten brick elements with twenty nodes, and steel bars were modeled as axial element embedded within brick concrete element.

Effect of radius To Span-length Ratio (R/L)

To investigate the effect of radius to span-length ratio, four reinforced concrete arched beams were analyzed numerically. Figure (10) shows the load deflection curve for those reinforced concrete arched beams which have different (R/L) ratio (R/L=2, 1.5, 1, and 0.7). From this figure, it can noticed that the ultimate load decreases when the decreases of (R/L) ratio. When the (R/L) ratio is increase, the subtended angle for arched beams will decrease and due to this decreasing in subtended angle the ultimate load will increase. This is occurring with constant span length of the arched beam.

Effect of Boundary Condition

To investigate the effect of boundary conditions on behavior of the reinforced concrete arched beams, three reinforced concrete arched beams with different boundary conditions were analyzed numerically.

Figure (11) shows the load-deflection curves at the point under the load for three reinforced concrete arched beams (simply, simply-fixed, and fixed supported beam). From this Figure, it can see that the collapse load for fixed support beam greater than other beams (simply and simply-fixed supported) by about 89% and

53% respectively and the deflection for simply supported beam is greater than simply-fixed and fixed supported beam.

Effect of (α_2) [The sudden loss of stress at instant of cracking]

To study the effect of (α_2) on the behavior of reinforced concrete arched beams. Three arched beams with different value of (α_2) (0.50, 0.75, and 0.90) were analyzed numerically. Figure (١٢) indicates that the increase of value (α_2) has significant effect on the behavior of arched beam.

Figure (12) shows that when value of (α_2) increases from 0.5 to 0.90, the ultimate load will increases about 7.5%, because the sudden loss ratio in normal stress at instant cracking will decreases, this decreasing causes increases in ultimate load.

Effect of compressive strength

The three high strength reinforced concrete arched beams and two normal strength reinforced concrete arched beams, are used to study the influence of the compressive strength on the ultimate loads. The behavior of the beams with low compressive strength of concrete is softer than those of concrete having higher strengths. Figure (13) show the response of the considered high strength reinforced concretes arched beams for different concrete compressive strength. Predicated ultimate loads for these five arched beams are also given in Table (4).

SUMMARY AND CONCLUSIONS

A nonlinear finite element analysis of high and normal strength reinforced concrete arched beams using a full three dimensional model have been presented. The main objectives of this study are to investigate the accuracy and efficiency of the computational finite element models in simulating the structural behavior of structures. The adopted material constitutive relationships are based on the incremental theory of plasticity of concrete in compression and the smeared crack representation of concrete in tension with an elastic-linear work hardening model used to simulate the behavior of reinforcement. Several parametric studies have been carried out in the current research to investigate the effect of some material and numerical parameters on the predicted behavior of the high and normal strength reinforced concrete arched beams.

Based on the finite element analysis carried out throughout the present work, the following conclusions are drawn:

The results obtained from the present finite element method show that the computational model adopted in this study is suitable for the prediction of load-deflection behavior of reinforced concrete arched beam under static loading. The comparison between the numerical and the available experimental results gave good agreement.

The ultimate load for fixed supported arched beam is greater than the ultimate load for simply-fixed supported arched beam by about 53 % and for simply supported arched by about 89 %.

The effect of the radius to span-length ratio (R/L) was noticed to have most pronounced effect on the load-deflection behavior of arched beam. It is found that the increases of the radius to span-length ratio increase the ultimate load and decrease in the ultimate deflection [when (R/L) increases from 0.7 to 2.0 the ultimate load increase of about 52%].

From the parametric studies carried out on arched beam, it can be concluded that the increase of (α_2) [The sudden loss of stress at instant of cracking] leads to the increase of the ultimate load by about 7.5 %.

The finite element analysis indicated that the increase on the concrete compressive strength of arched beam from (19 MPa) to (80 MPa) lead to increase in the ultimate load by about (71%).

REFERENCES

[1]. ACI Committee 363," State of the Art Report on High Strength Concrete" (ACI 363 R-84), American Concrete Institute, Detroit 1984, pp.48.

[2]. Al-Shaarbaf , I.A.S ., (1990) "Three-Dimensional Nonlinear Finite Element Analysis of Reinforcement Concrete Beams in Torsion", Ph.D Thesis, University of Bradford.

[3]. Bradford, M. A., Wang, T., Pi, Y.-L., and Gilbert, R. I. (2007). "In-plane stability of parabolic arches with horizontal spring supports. Part 1: Theory." J. Struct. Eng., 133(8), pp 1130–1137.

[4]. Carrasquillo, R. L., Nilison .A H., and Slate, F.O., (1981),"Properties of High Strength Concrete Subjected to Short- Term Loads", ACI Journal Vol.78, No.3.

[5]. Cook, R.D., (1974), "Concept and Application of Finite Element Analysis", John Wiley and Sons, Inc., New York.

[6]. Dickie, J. F., and Broughton, P. (1971). "Stability criteria for shallow arches." J. Engrg. Mech. Div., 97(3), pp 951–965.

[7]. Gjelsvik, A., and Bodner, S. R. (1962) "Energy criterion and snap buckling of arches." J. Engrg. Mech. Div., 88(5), pp87–134.

[8]. Gopalaratnam, V.S. and Shah. "Softening Response of Plain Concrete in Direct Tension", ACI Journal, Vol. 82, No.3, pp, 310-323.

[9]. Hadi, W.K.,(2002),"Elastic-plastic analysis of reinforced concrete shallow arched frames using curved beam element ", Msc. Thesis, University of Babylon.

[10]. Isenberg, J., (1993)"Finite Element Analysis of Reinforced Concrete Structures II", ASCE, NewYork ,NY.

[11]. Jain,O,P., (1980),"Ultimate strength of reinforced concrete arches", ACI Journal , Vol. 32, No.6, December,pp.697-713.

[12]. Kupfer,H.B., Hilsdrof, H.K., and Rusch, H., (1969),"Behavior of concrete under Biaxial Stresses",J. Am. Concr. Inst, Vol. 66, No.8, August, pp.656-666.

[13]. Marzouk ,H.M., and Hussein ,A., (1990), "Properties of High-Strength Concrete at low Temperature", ACI Materials Journal , Vol. 87, Np.2, pp.167-171.

[14]. Mehta, P.R.,(1986),"Concrete Structures Proposes and Materials", Prentice – Half , New Jersey , pp. 450.

[15]. Mosheer, Kh. A., 2005, "Nonlinear Finite Element Analysis of Reinforced Concrete Deep Beams With Openings" Msc. Thesis, University of Babylon. . Park.R. and Gamble.W.L.,(2000),"Reinforced Concrete Slabs ".Wilcy , NewYourk.

[16]. Rubin, M. B.(2004),"Buckling of elastic shallow arches using the theory of a Cosserat point" J. Eng. Mech., 130(2), pp216–224.

[17]. Schreyer, H. L., and Masur, E. F. (1966). "Buckling of shallow arches" J. Engrg. Mech. Div., 92(4),pp 1–17.

[18]. Simitses, G. J. (1976). "An introduction to the elastic stability of structures", Prentice-Hall, Englewood Cliffs, N.J.
[19].. Timoshenko, S. P., and Gere, J. M. (1961)," Theory of elastic stability" McGraw-Hill, New York.
21. Wang ,P.T., Shah , S.P., and Naaman ,A.E., " Stress-Strain Curves of Normal and Light Weight Concrete in Compression" ACI Journal, Nov. 1978, pp. 603-611.
[20]. Wang, P. T.,Bradford, M. A., , Pi, Y.-L., and Gilbert, R. I. (2007). "In-plane stability of parabolic arches with horizontal spring supports. Part 2: Theory." J. Struct. Eng., 133(8), pp1138–1145.
[21]. Piero Marro. "Bending and Shear Tests Up to Failure of Beams Made with High-Strength Concrete" Symposium in Stavanger ,Norway , 1987.pp.183.

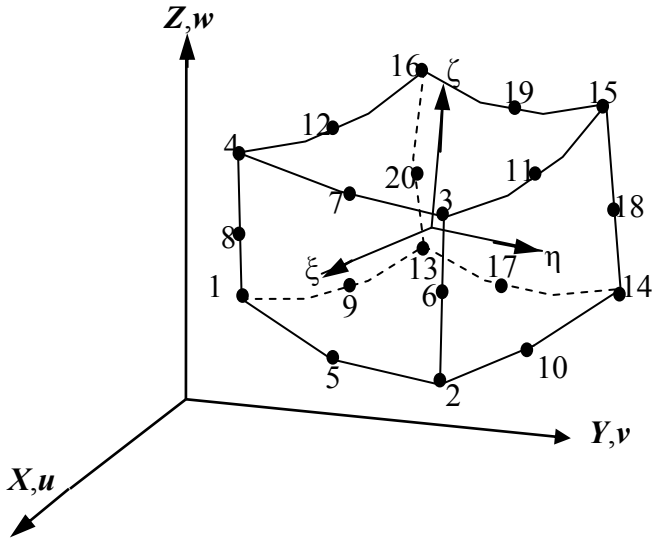

Figure (1) twenty nodes Brick Element.

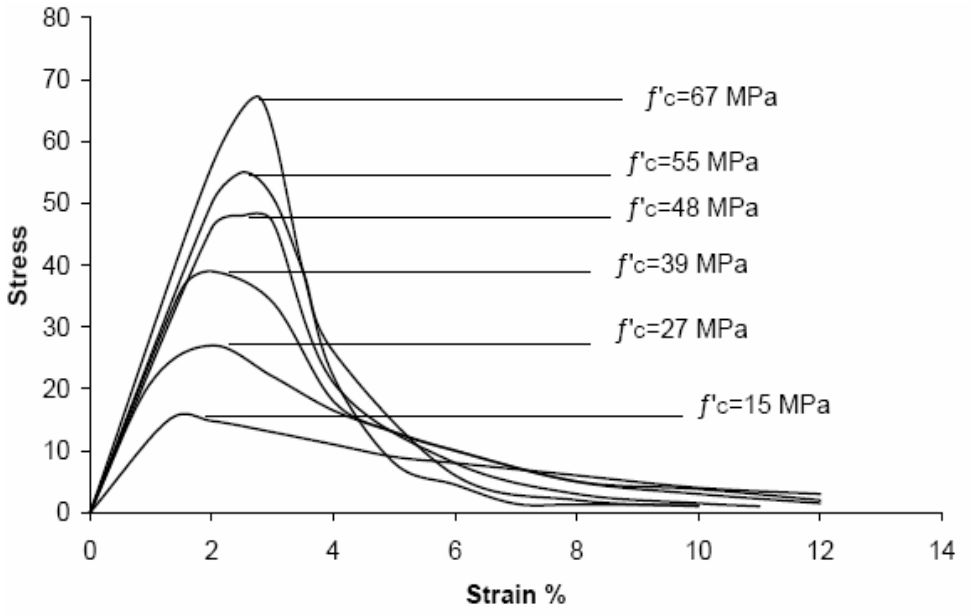

Figure (2) Compressive stress-strain curve for different grades of concrete[20].

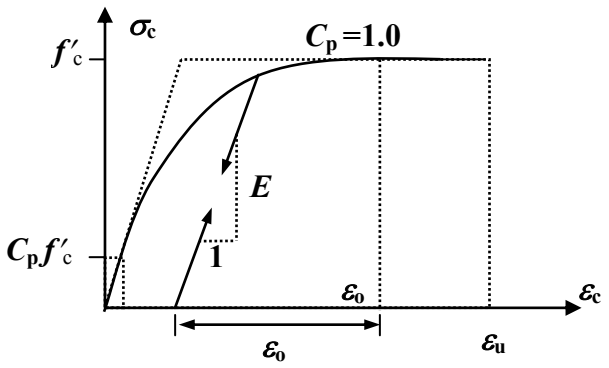

Figure (3) Uniaxial Stress-Strain Curve for Concrete [12].

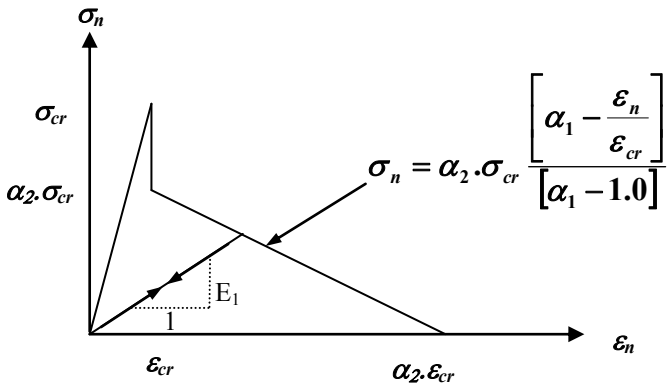

Figure (4) Post Cracking Model for Concrete[12]

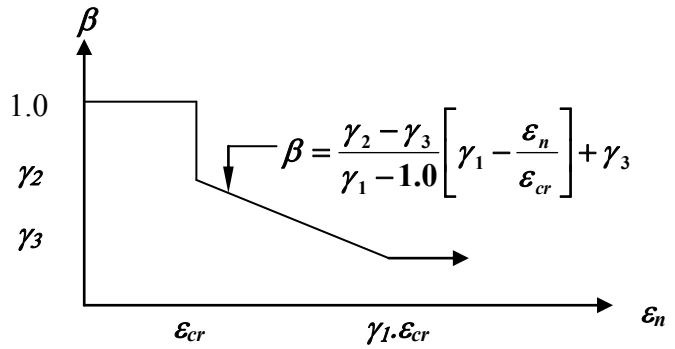

Figure (5) Shear Retention for Concrete [12].

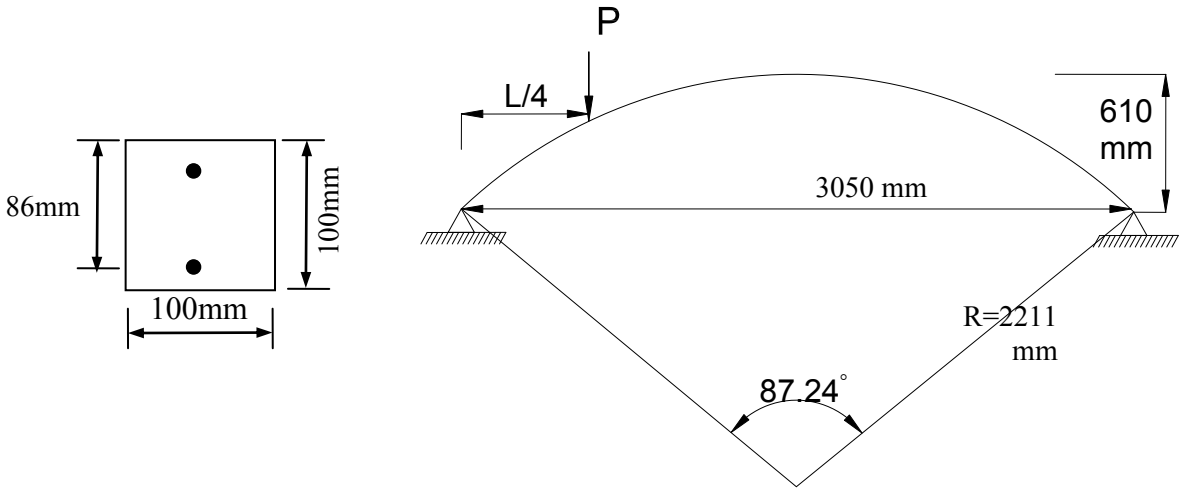

(a) beam geometry, loading arrangement and reinforcement details.

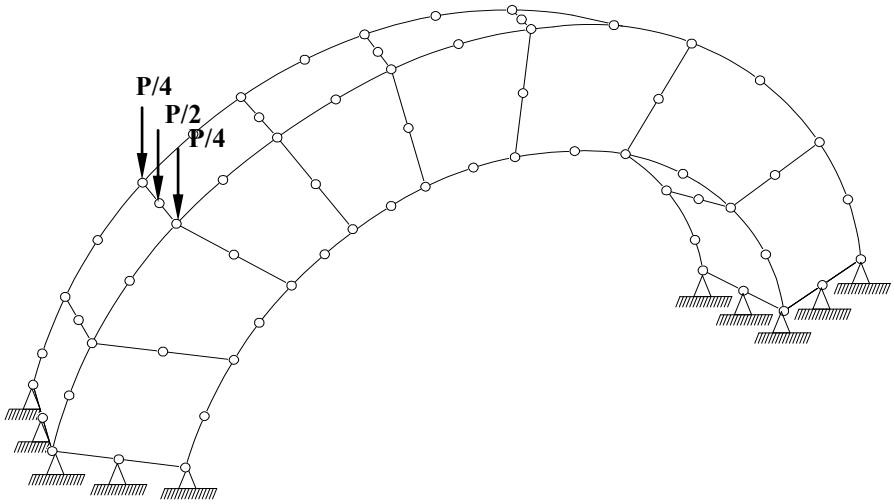

(b) Finite Element idealization of beam

Figure (6) Simply supported reinforced concrete arched beam.

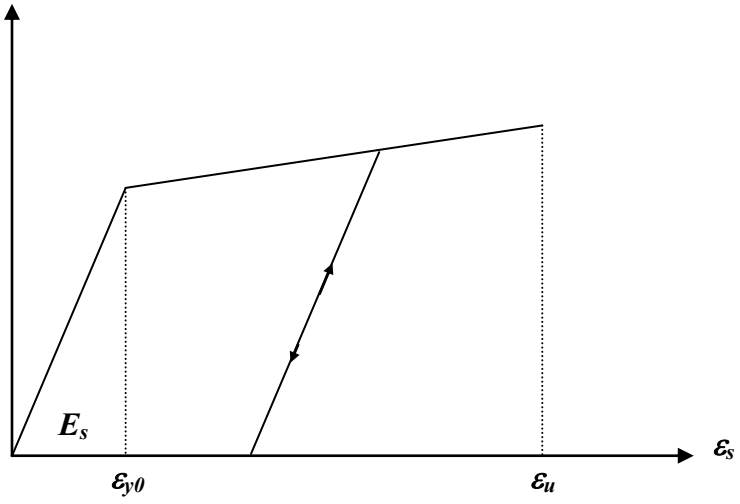

Figure (7) Stress-Strain Relationship of Steel Bars Used in the Analysis.

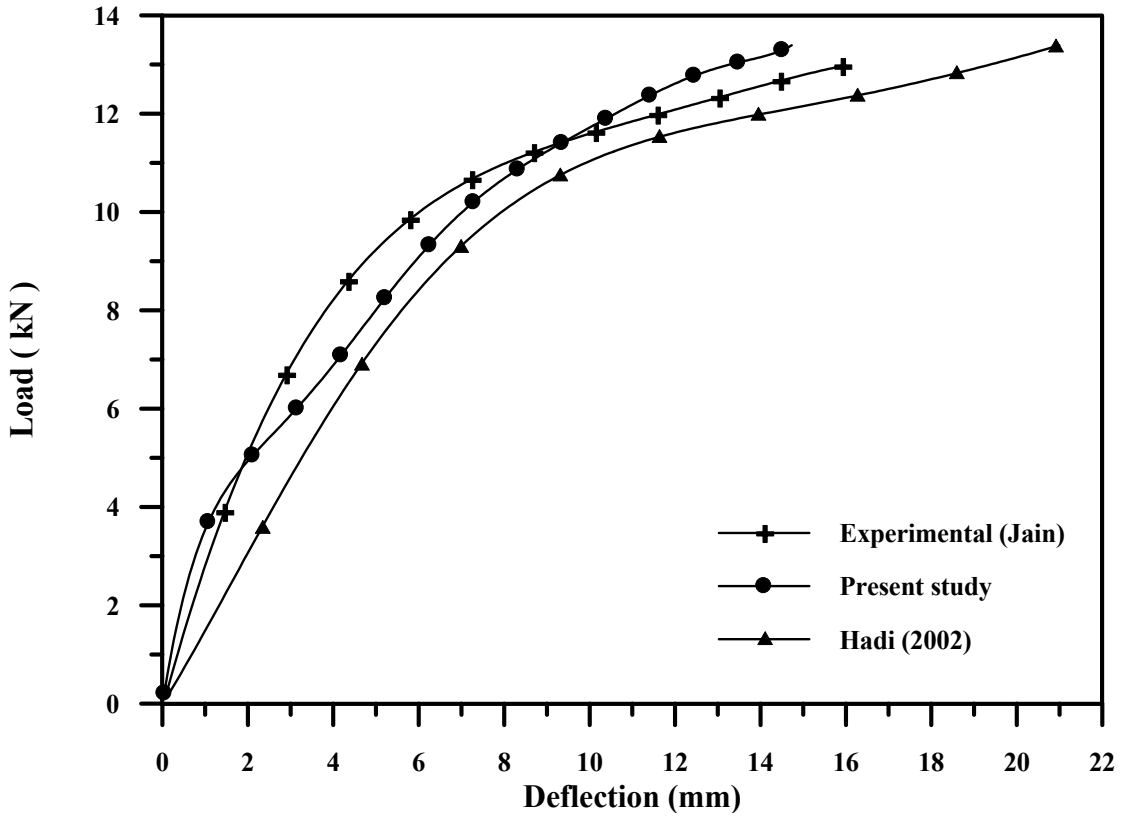

Figure (8) Load-deflection curves under point load of simply supported arched beam with subtended angle 87.24° (Example No.1).

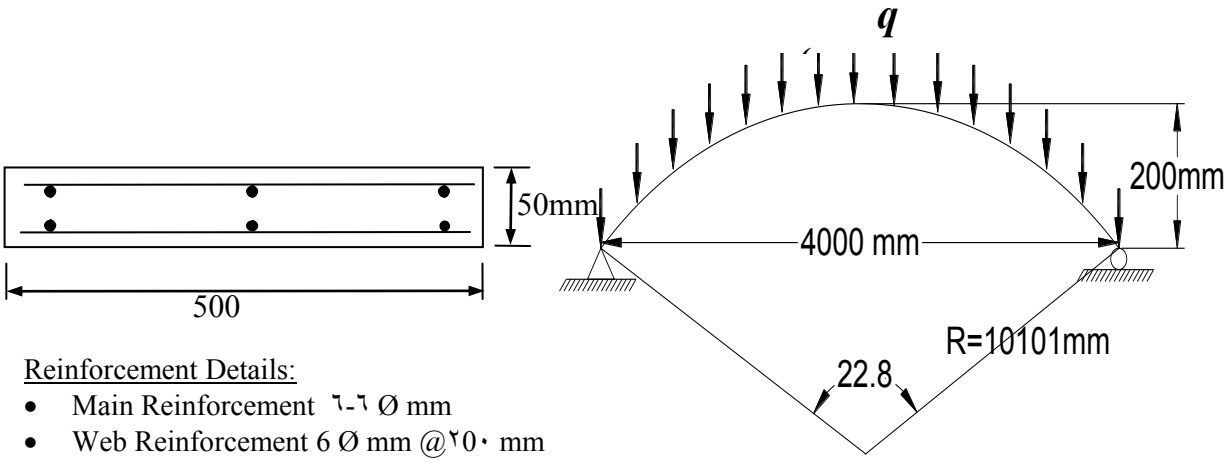

Reinforcement Details:

- Main Reinforcement ٦-٦ Ø mm
- Web Reinforcement 6 Ø mm @٢٥٠ mm

(a) Beam geometry, loading arrangement and reinforcement details

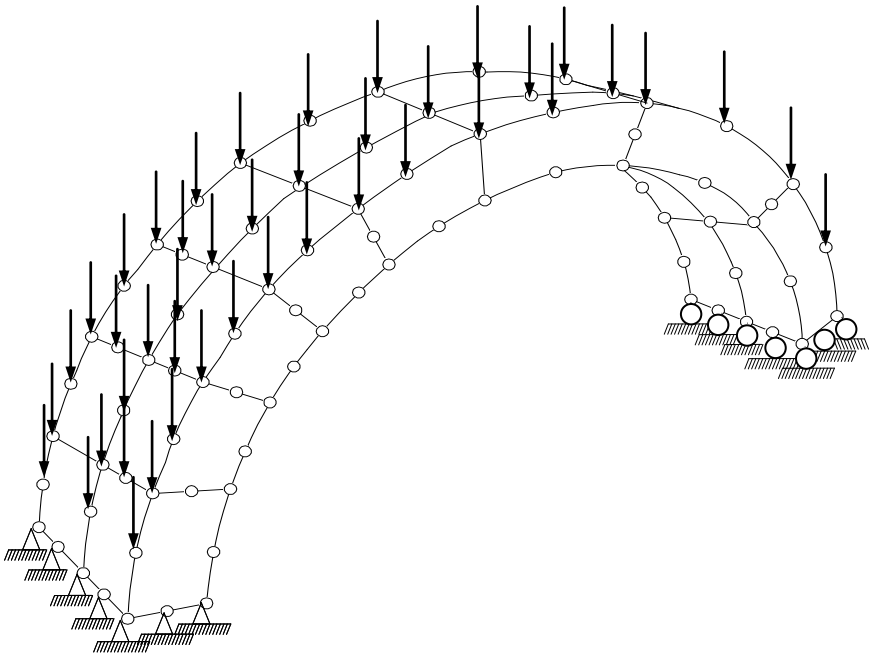

(b) Finite Element idelization of beam (16 brick elements)

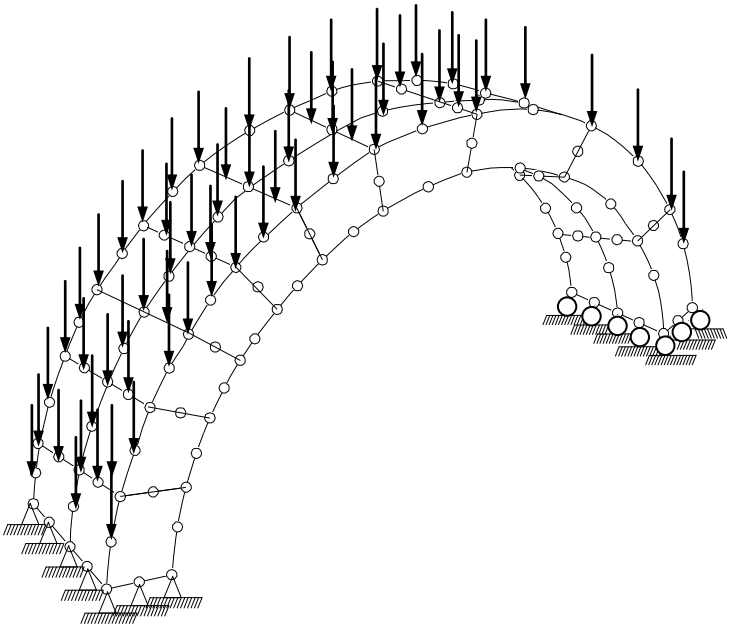

(c) Finite Element idelization of beam(20 brick elements)

Figure (9) Roller-pin Supported Reinforced Concrete Arched Beams.

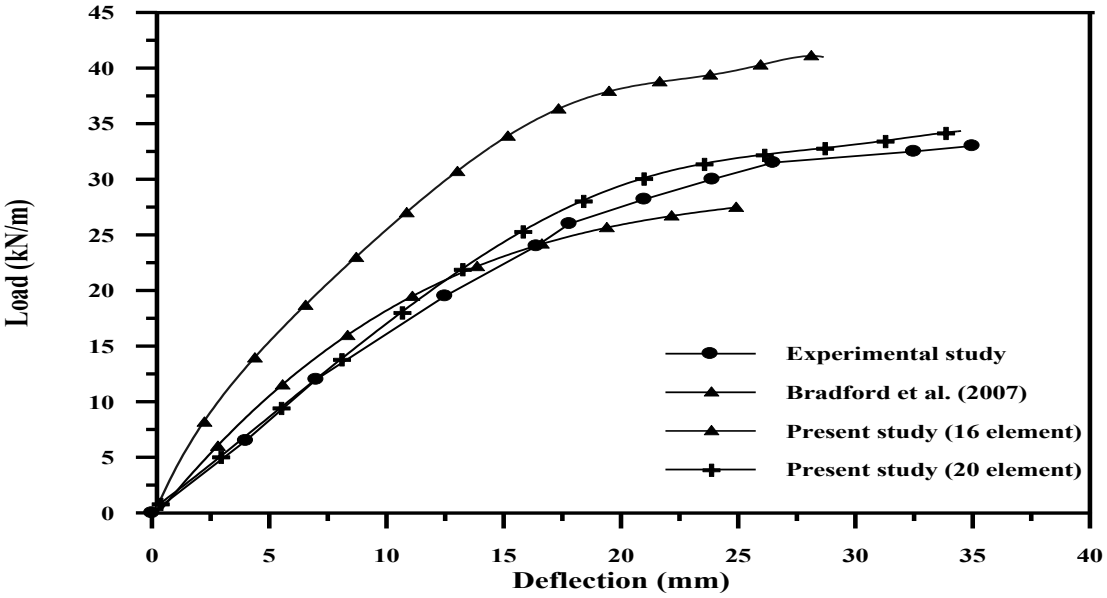

Figure (10) Load-deflection curves at mid span of Roller-pin Supported Arched Beams with subtended angle 22.8° (Example No.2).

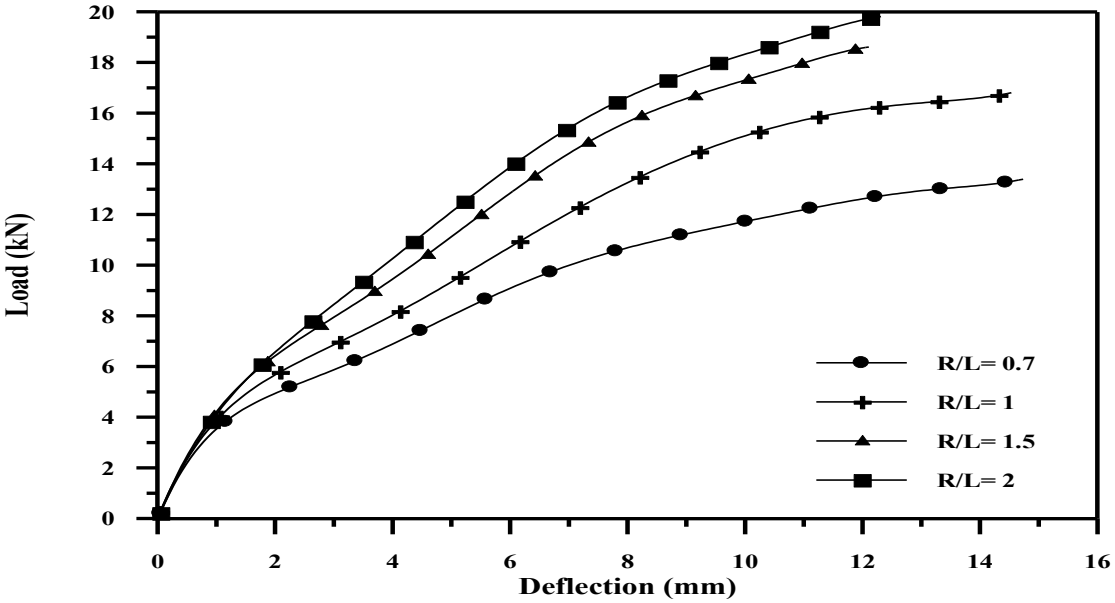

Figure (11) Load-deflection curve under point load for arched beam with Various radiuses to span-length ratio(R/L).

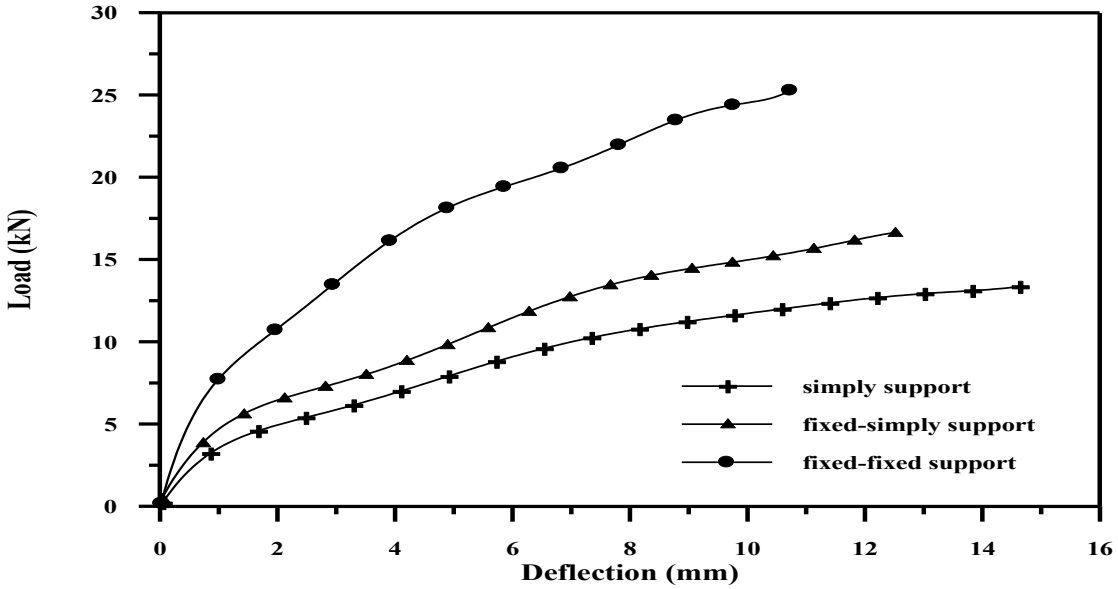

Figure (12) Load-deflection under point load for curved beam with various

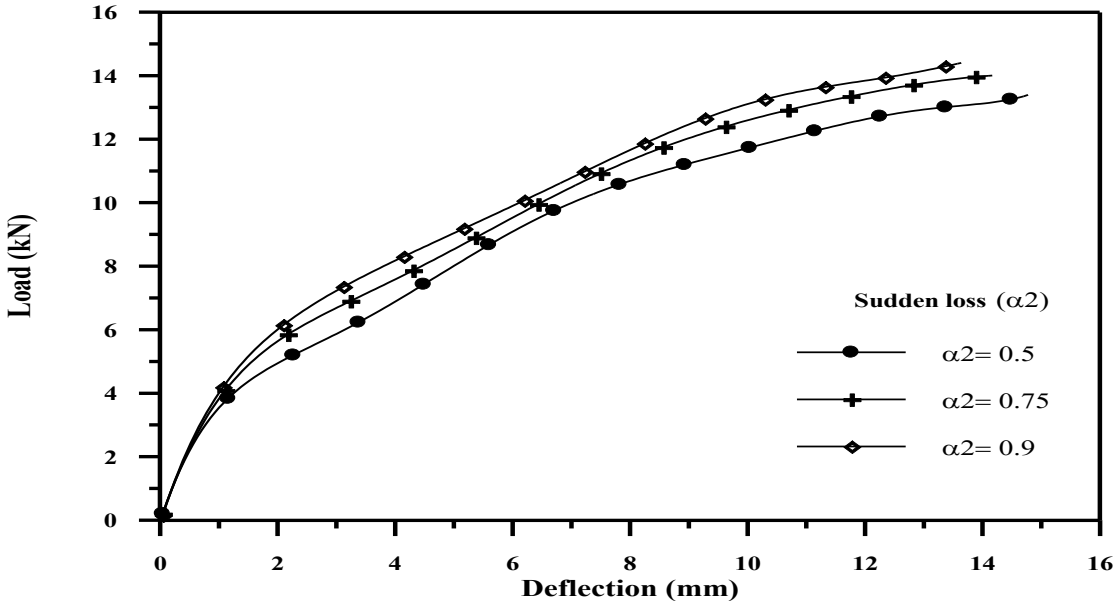

Figure (13) Load-deflection under point load for arched beams with various (α_2).

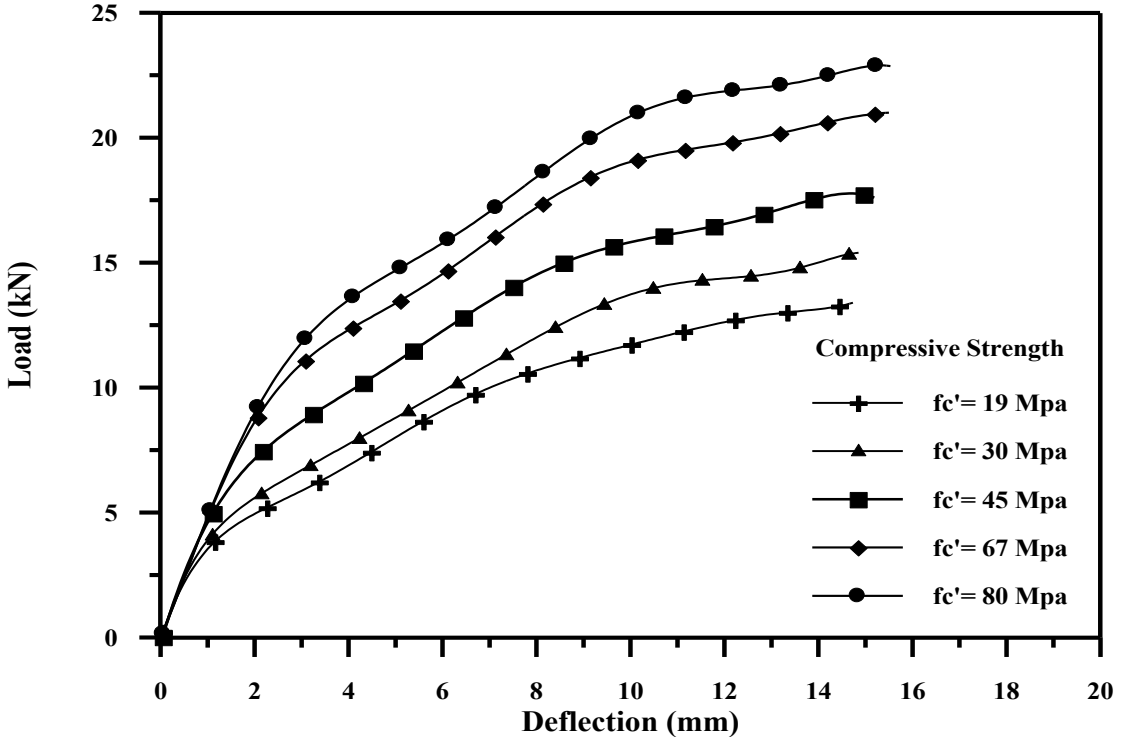

Figure (14) Load-deflection under point load for arched beams with high and normal strength

Table (1) Shape Functions of the Quadratic Twenty Node Brick Element [5]

Location	ξ	η	ζ	N_i (ξ, η, ζ)
Corner nodes	**±1**	**±1**	**±1**	**$(1+\xi\,\xi_i)(1+\eta\,\eta_i)(1+\zeta\zeta_i)\,(\xi\,\xi_i+\eta\,\eta_i+\zeta\,\zeta_i-2)/8$**
Mid-side nodes	**0**	**±1**	**±1**	**$(1-\xi^2)(1+\eta\,\eta_i)(1+\zeta\,\zeta_i)/4$**
Mid-side nodes	**±1**	**0**	**±1**	**$(1-\eta^2)(1+\xi\,\xi_i)(1+\zeta\,\zeta_i)/4$**
Mid-side nodes	**±1**	**±1**	**0**	**$(1-\zeta^2)(1+\xi\,\xi_i)(1+\eta\,\eta_i)/4$**

Table (2) Material properties and additional parameters of simply Supported reinforced concrete arched Beam Example No.1

	Material properties and material parameters	Symbol	value
Concrete	Young's modulus	E_c(N/mm^2)	265٠٠
	Compressive strength	f_c'(N/mm^2)	19
	Tensile strength *	f_t(N/mm^2)	2.3
	Poisson's ratio	**ν**	0.17
	Uniaxial crashing strain **	ε_{cu}	٠.٠٠٣
Steel	Young's modulus	E_s(N/mm^2)	200000
	Yield stress for main reinforcement	f_y(N/mm^2)	483
Tension stiffening parameter	Rate of stress release**	α_1	20
	Sudden loss of tension stiffness at the instant of cracking **	α_2	٠.٥
Shear retention parameters	Rate of decay of shear stiffness **	γ_1	١٠.٠
	Sudden loss of shear stiffness at the instant of cracking **	γ_2	٠.٥
	Residual shear stiffness due to the ** dowel action	γ_3	٠.١

* Assumed by Jain[11].
** Assumed in the present study.

Table (3) Material properties and additional parameters of simply Supported reinforced concrete arched Beam Example No.2.

	Material properties and material parameters	Symbol	value
Concrete	Young's modulus	E_c(N/mm^2)	253٠٠
	Compressive strength	f_c'(N/mm^2)	34
	Tensile strength *	f_t(N/mm^2)	3.4
	Poisson's ratio	ν	0.17
	Uniaxial crashing strain **	ε_{cu}	٠.٠٠٣
Steel	Young's modulus	E_s(N/mm^2)	200000
	Yield stress for main reinforcement	f_y(N/mm^2)	400
Tension stiffening parameter	Rate of stress release **	α_1	20
	Sudden loss of tension stiffness at the instant of cracking **	α_2	٠.٥
Shear retention parameters	Rate of decay of shear stiffness **	γ_1	١٠.٠
	Sudden loss of shear stiffness at the instant of cracking **	γ_2	٠.٥
	Residual shear stiffness due to the ** dowel action	γ_3	٠.١

Table (4) Predicted ultimate load for the reinforced concrete arched beams with different values of compressive strength.

Compressive strength f_c'(MPa)	**Predicted ultimate load (** kN **)**
19	**13.4**
30	**15.4**
45	**17.6**
67	**21**
80	**22.9**